Spectroscopic Diagnostics of AC Discharge in Magnetron Sputtering System

Zahraa M. Hasan
Qusay A. Abbas

Department of Physics, College of Science, University of Baghdad, Baghdad, IRAQ

This paper investigates the effect of the AC discharge frequency, and the magnetic field on the discharge characteristics of a cylindrical magnetron sputtering device operating at constant argon pressure. The AC argon discharge was produced by applied high voltage alternating 10 kV with frequencies 7 and 9 kHz. The optical emission spectroscopy technique was used to determine the effect of source frequency and magnetic field on emission spectra, glow discharge regions and other discharge parameters (such as T_e, n_e, λ_D and N_D). The emission spectra of an argon discharge at both source frequencies indicate that the emission intensity of Ar I and Ar II increases as the coil current increases. The emission intensities of the peak lines of Ar I and Ar II increase with increasing source frequency. An optical emission spectrometer was used to diagnose the effect of source frequency and magnetic field on the AC discharge properties using the Boltzmann plot method, the electron temperature was determined. The electron number density was calculated using Stark broadening. The data showed that the electron temperature, electron density, Debye length, and plasma parameters increased with increases in the coil current at both source frequencies. Moreover, the increase in source frequency causes increases in all discharge parameters.

Keywords: Boltzmann plot; AC discharge; cylindrical magnetron sputtering; Stark broadening
Received: 01 September 2023; **Revised:** 25 September 2023; **Accepted:** 02 October 2023

1. Introduction

Magnetron sputtering is one of the most commonly used methods of vacuum deposition, and it can be used to deposit metals and nonmetals on a wide variety of substrate materials [1-2]. Magnetron sputtering systems (MSS) are frequently utilized in the process of depositing altering coatings on the surfaces of materials. This is due to the fact that MSS produces coatings of high quality that expose an extensive range of functional features [3] .In the 1960s and 1970s, the magnetron sputtering method was developed. Since then, it has become the most important part of plasma sputtering applications. Magnetron sputtering deposition techniques are most frequently employed for thin film deposition and surface engineering procedures [4]. In the 1970s, Cormia et al. used mid-frequency AC power to help deal with the formation of a compound layer and the subsequent charging of the target [5]. By the middle of the 1980s, experts like Este and Westwood had used a dual magnetron method to greatly improve the rate of deposition and efficiency of this method [6]. Este and Westwood pioneered the use of twin magnetrons in 1987, which were developed by Scherer in 1991 and Glocker in 1993 [7]. Mid-frequency AC magnetron sputtering is similar to the DC process mentioned above, except that the cathode and anode switches are switched every half cycle [8]. Plasma production is regarded topic since it is a highly effective method for material fabrication and post-treatment. Glow discharge as an important plasma is a partially ionized gas composed of electrons, positive ions, negative electrons, and significant quantities of neutral species. It is thought to be one way to create plasma at pressure constant. It is simple to produce glow-discharge plasma using a high-voltage electrical discharge and a constant pressure gas system [9].This can be done using DC, AC or more usually high frequency AC. An electric potential is applied between two electrodes to produce an AC glow discharge. The high electrical potential of 10 kV is more than enough to produce plasma through the process of breakdown. This also results in strong emission due to the interaction of excited atoms. In comparison to conventional procedures, sputtering offers significant advantages. Studies were done on the characteristics of sputtering plasma under various discharge settings [10-11]. Diagnostics are the main focus of plasma study right now. Important plasma factors, such as chemical composition, plasma species, plasma density, plasma potential, plasma temperature, and the distribution of electron and ion energy [12-13]. To determine plasma properties, plasma diagnostic techniques such as the Langmuir probe, optical emission spectroscopy (OES), mass spectroscopy, and microwave interference can be used [14-16]. Due to its ease of use and lack of plasma disruption, OES is a useful tool for studying glow discharge [17]. The emission of plasma radiation is highly dependent on plasma characteristics and gas composition [18].

In the present paper, the influence of the magnetic field and AC discharge frequency on the argon discharge characteristics parameters of cylindrical magnetron sputtering system at constant pressure will investigate in more details.

2. Theoretical Description of Discharge Parameters

The electron temperature (T_e) is one of the most important plasma conditions. Te can be calculated using the Boltzmann diagram method, as displayed below [19-23].

$$\mathrm{Ln}\left(\frac{I_{ji}\lambda_{ji}}{g_j A_{ji}}\right) = \left(-\frac{E_{K,Z}}{K_B T_e}\right) + \ln\left(\frac{hcL_{nz}}{4\pi p_z}\right) \quad (1)$$

Here Z represent the variables ionization state, h is Planck's constant, c is light speed, K_B is Boltzmann constant, j is the highest energy level, i is lower energy level, λ_{ji} is the wavelength corresponding to the transmission between level j and level I for the same ionization degree, Aji the transition probability corresponds to transition from I to j, I_{ji} is the intensity of transition from I to j, P_Z is the species partition function in ionization stage Z, and g_j is a statistical weight. The electron temperature was calculated by plotted the left-hand side of equation (1) against the higher-level energy of the species in the Z ionization phase in eV unit.

There are many fundamental line broadening (Stark broadening, Doppler broadening, and pressure broadening) which can occur in the plasma. A stark broadening can also be used to calculate the electron number density as [24-32].

$$n_e(cm^{-3}) = \left[\frac{\Delta\lambda}{2\omega_s(\lambda,T_e)}\right] N_r \quad (2)$$

Where λ_D is the full width at half maximum of the line, ω_s is the electron impact value that can be found in the standard tables, and Nr is the density of reference electrons number density which equal to 10^{16} cm^{-3} for neutral atoms and 10^{17} cm^{-3} for single-charged ions [33-34].

Debye length is calculable using the formula [35-44].

$$\lambda_D = \left(\frac{\varepsilon_\circ k_B T_e}{e^2 n_e}\right)^{\frac{1}{2}} \quad (3)$$

where k_B denotes the constant of Boltzmann.

anyway, The plasma parameter (N_D), which stands for the number of charged particles contained within the Debye sphere and is calculable as a function of the electron number density as well as the electron temperature, can be expressed as [45-49].

$$N_D = \frac{4}{3}\pi n_e \lambda_D^3 \cong 1.38 \times 10^6 \frac{[T_e(k^0)]^{3/2}}{[n_e(m^{-3})]^{1/2}} \quad (4)$$

3. Experimental Part

Figure (1) schematic the diagram of the alternating current magnetron sputtering system that used in this work. This system consists of stainless steel vacuum chamber, two aluminum coaxial cylindrical electrodes, D.C. solenoid magnetic coil, pumping system, and A.C. power source were utilized in vacuum chamber to generated argon discharge. The outer cylindrical (wall of the chamber) which represent the powered electrode has 25 cm in diameter and 22cm of length. The inner cylinder (ground electrode) has 3cm in diameter and 18 cm in length. Two A.C. frequencies of 7 and 9 kHz are supplied by an A.C. source to coaxial cylindrical electrodes in the absence and presence of a magnetic field in order to generate A.C. discharge in argon gas (99.9% impurity) at 0.2 torr constant pressure. D.C. magnetic solenoid coil with turns, inner diameter, maximum current is 6A, and length 22cm was used to confine the plasma particles in the central region with strong magnetic field T and a maximum coil current 6Amp. Double stage rotating pump model CIT-ALCATEL Annecy (made in France) was used to evacuate to a base pressure of 0.2 Torr. While the argon pressure was measured using a Pirani gauge (made in England), the A.C. discharge was produced by applied rms. voltage of 10 kV with different frequency 7 and 9 kHz between two coaxial cylinders. A.C. discharge images were captured by a high-resolution digital canon camera with a variety of settings. The plasma emission spectra were diagnostics by using an optical emission spectrometer THORLAB model (made in Germany) in the wavelength range 320–740 nm In relation to the plasma column, the spectrometer was positioned at a 45-degree angle. The spectra data were calibrated using NIST database software to determine the plasma parameters.

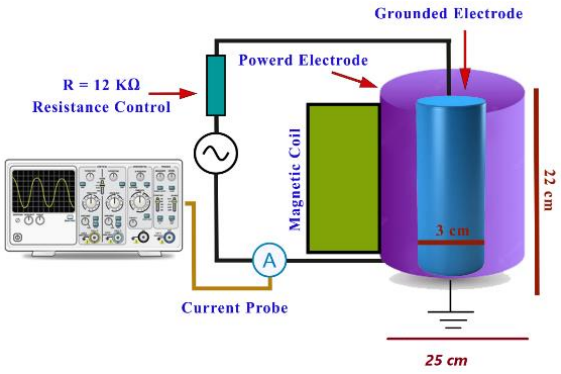

Fig. (1) The inverted configuration sputtering diagram for a cylindrical magnetron

4. Results and discussion

The influence of A.C. frequency on the emission spectra of plasma in the inverted cylindrical magnetron configuration at constant argon gas pressure over the wavelength range of 320–740 nm are illustrated in figures (2) and (3). The spectra of these figures display five emission peaks of neutral argon (ArI) at 419.83170, 687.12890, 696.54300, 706.87350, and 738.39800 nm, in addition to five ionic emission peaks of argon (ArII) located at 361.18130, 427.75280, 434.80640, 476.48640, and 487.98630 nm. As well as, It is clear from these data that an increase in the number of inelastic collisions that take place in the plasma as a result of plasma confinement leads to an increase in the emission peak intensity of all emission peaks (both atomic and ionic peaks), and this rise occurs in conjunction with an increase in the coil currents.

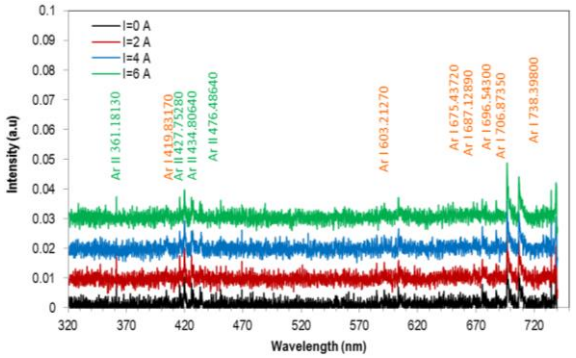

Fig. (2) Effect of the coil current on the optical emission spectra of AC argon discharge for frequency of 7kHz at 0.2 torr

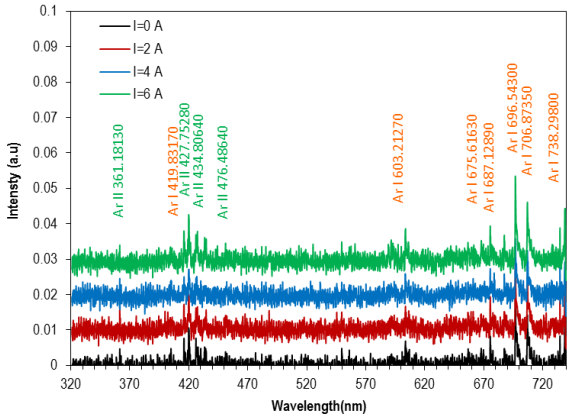

Fig. (3) Effect of the coil current on the optical emission spectra of AC argon discharge for 9 kHz at 0.2 torr

By applying of alternating voltage of about 10 kV, the AC normal glow discharge was established in argon gas. The schematic photography shown in Figure (4) shows the effect of coil current on regions of normal glow discharge at source frequencies of 7 and 9 kHz, respectively, with a constant pressure of 0.2 torr. Many features can be noted from these figures which can be detected as, the normal glow structure in low frequency alternating current discharge was similar to that produced in the direct current discharge. When the magnetic field increases (caused by increases in the coil current), the powered region (powered fall) is compressed. The positive column and grounded regions (grounded fall) grow, and the negative glow transforms into a thin layer of intense luminosity. The presence of the magnetic and electric fields together causes the electrons to follow a helical path around the magnetic field lines, which increases the ionization collisions and maintains the discharge with argon atoms close to the powered electrode. This variation in the glow discharge structure with an increase in the magnetic field can be explained in this way. Therefore, the electrons were moves a shorter distance along the axis of the powered dark space. Thus, the length of the powered dark region is reduced. On the other hand, the increases of the positive column region and grounded fall are due to the constrain of the electron diffusion (i.e. the electron losses are reduced) perpendicular to magnetic field direction. The comparison of figures (4) demonstrated that all normal glow discharge region at source frequency 9 kHz are more luminous comparable to source frequency 7 kHz caused by the electrons gain more energy from applying electric field at the frequency source 9 kHz.

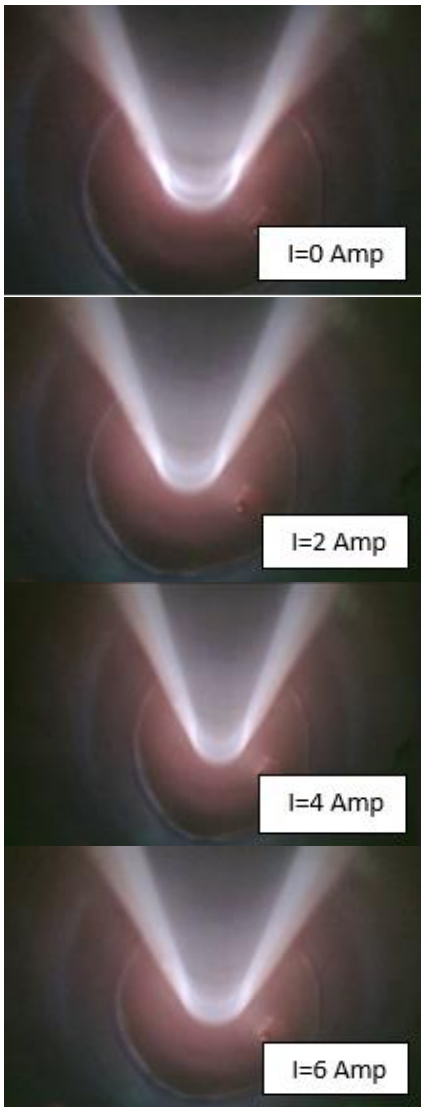

(F=7kHz)

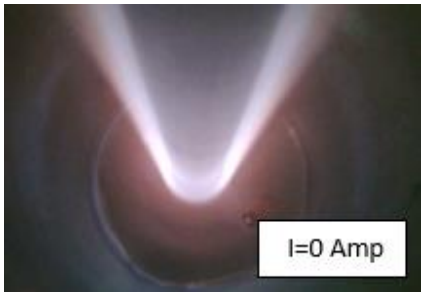

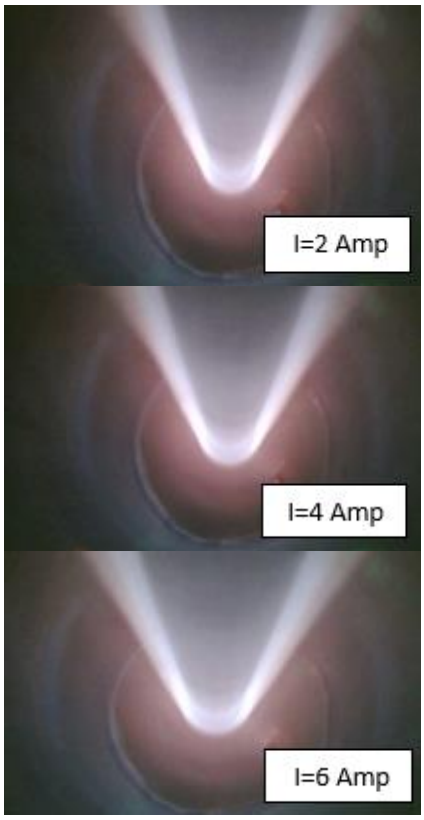

(F=9kHz)

Fig. (4) Schematic the photography of for AC glow structure at constant pressure of 0.2 torr for different coil currents with frequency (7,9kHz)

Figure (5) shows how the frequency of the AC source affects the change in discharge voltage as a function of the coil current. The data detected the discharge voltage has approximately a constant value with increasing of the coil currents. When the source frequency increases from 7 kHz to 9 kHz, the discharge voltage was raised. The increasing of the discharge voltage with source frequency is attributed to increasing of the space charge effect caused by increasing of ionization collisions of electrons with neutral atoms which causes to increasing of the voltage that needed to maintain the discharge.

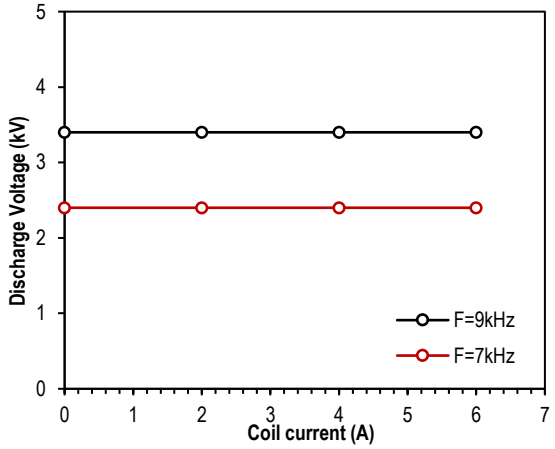

Fig. (5) Influence of Ac source frequency on the variation of the voltage discharge versus coil currents

Figure (6) shows how the AC source frequencies affect how the discharge current changes as a function of the coil currents. This figure shows that, at higher rates of frequency (9 kHz), the discharge current increases with increasing coil current (increasing plasma confinement). The increase of plasma confinement means that increase of ionization collisions of electrons with neutral atoms.

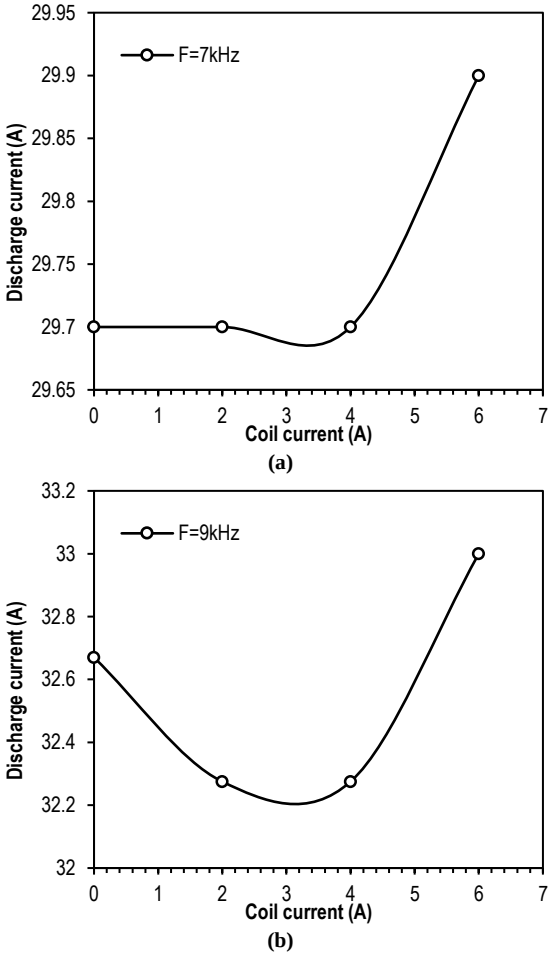

Fig.(6) The variation of discharge current as a function of coil current at different AC source frequencies from (a) 7kHz (b) 9 kHz

The electron temperature is one of the most important basic plasma factors that is used to describe the state of the plasma medium. Electron temperature (T_e) controls plasma activation and ionization. To compute Te, assuming the plasma is in local thermodynamic equilibrium and the Boltzmann distribution is applicable to the number of excited atoms, which was computed using the Boltzmann plot method (Eq. 1). By using Eq. (1) and data that listed in table (1), the electron temperature was calculated.

Figures (7) and (8) The Boltzmann plots for the post-discharge configuration using specific atomic argon lines (Ar I) at various coil currents and source frequencies are shown.

Table (1) Shows how Ar-I standard lines are used to calculate electron temperatures and their properties [50]

λ(nm)	Ag(S^{-1})	Ei(ev)	Ej(ev)	Ion
419.83170	2.57×10^{6}	11.62359272	14.57594878	Ar I
687.12890	8.34×10^{6}	12.90701530	14.71089810	Ar I
696.54300	1.9×10^{7}	11.54835442	13.32785705	Ar I
706.87350	6.0×10^{6}	13.09487256	14.84836899	Ar I
738.39800	4.2×10^{7}	11.62359272	13.30222747	Ar I

As well as, the electron number density (n_e) was calculated using the Stark broadening effect (Eq. (2)). The influence of AC frequency on the variation of electron temperature and electron number density with increasing coil current (increasing magnetic field) of the post-cylindrical magnetron sputtering device is illustrated in Fig. (9). According to the graph, increasing the coil current induces an increase in both the electron number density and the electron temperature at all frequencies under consideration. The increases in electron number density with increasing coil current can be attributed to the increased inelastic collision of the electrons with argon atoms caused by magnetic confinement, whereas the increases in electron temperature with increasing coil current (increases in the magnetic field) can be attributed to the magnetic confinement of the electrons in the region close to the surface of the powered electrode surface where the electric field is strongest.

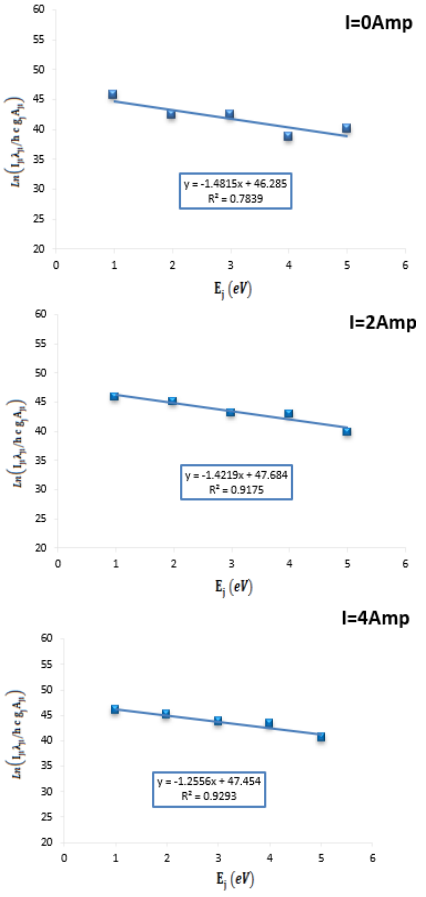

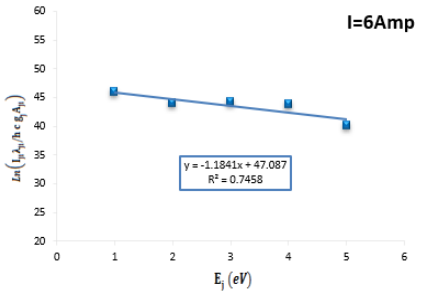

Fig. (7) Boltzmann plots for post-discharge configuration utilizing selected atomic argon lines (ArI) at various coil currents and a 7 kHz frequency

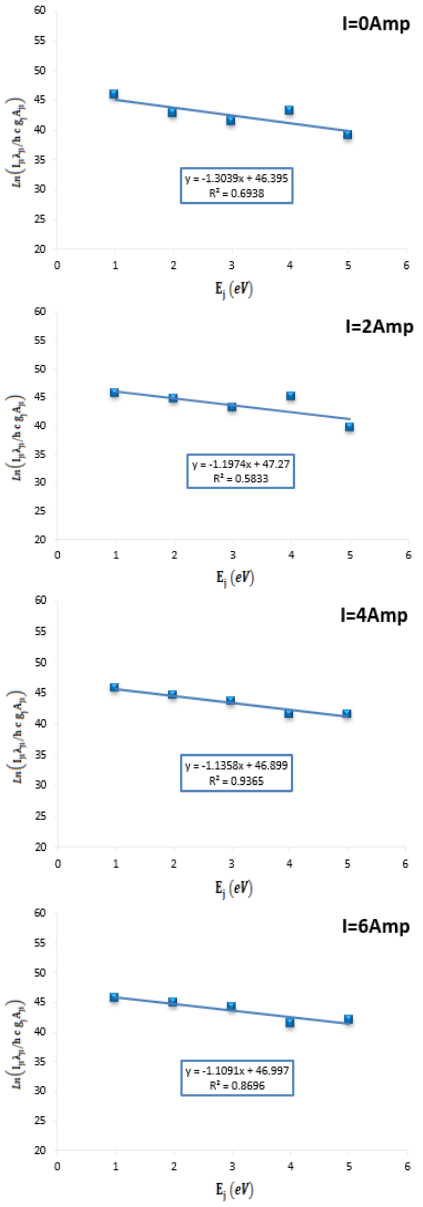

Fig. (8) Boltzmann plots for post-discharge configurations with selected atomic argon lines (ArI) at various coil currents at a frequency of 9 kHz

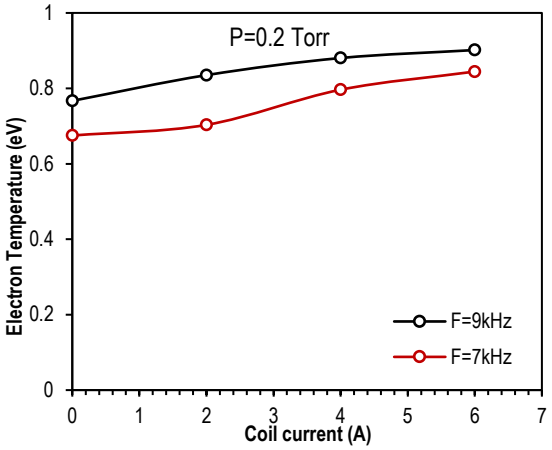

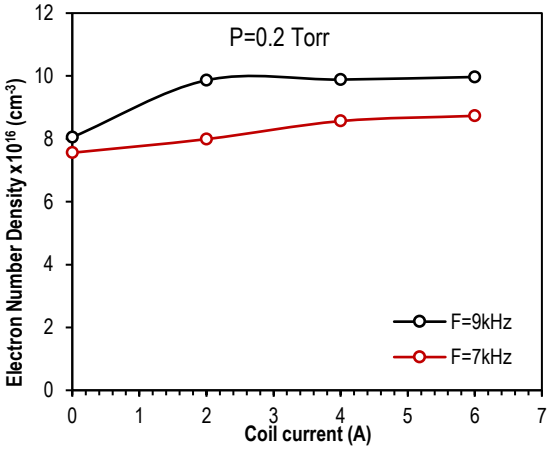

Fig.(9) Influence of AC frequency on the variation of electron temperature and electron number density with increasing coil current in a post-cylindrical magnetron sputtering device

Another fundamental discharge parameter which calculated in this paper is Debye length (used Eq. 3). Figure (10) found that the Debye length changed depending on how the coil current worked for both of the AC frequencies under study. One can observed from this figure the Debye length was increase with increases of coil current. This results mean that the powered electrode sheath that formed surrounded the powered electrode is reduced with increases of the coil current. This impact increases the volume of plasma. Due to confinement, the presence of the magnetic field causes a reduction in plasma volume.

The plasma parameter (N_D) also calculated according to data that listed in table (2) and equation (4), the variation of N_D with coil current in two AC source frequencies are tabulated in table (2). The data detected the increases of number of the charge particles caused by increasing of ionization collisions with increasing of coil currents. Furthermore, the increasing of AC frequency from 7 to 9 kHz causes to production more charge particles due to a raising of the absorbed energy by the electrons.

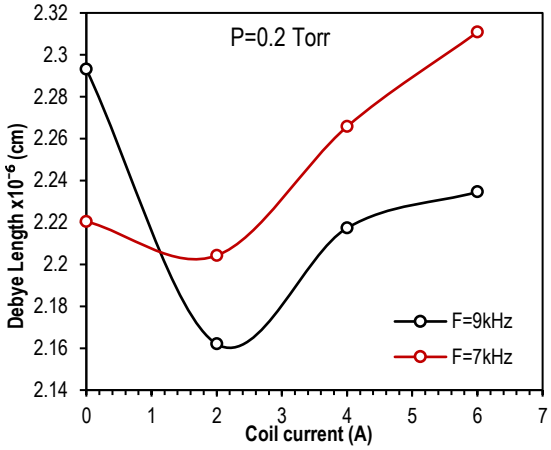

Fig. (10) The difference (λ_D) in constant gas pressure between the presence and absence of B

5. Conclusion

This study examined how AC source frequency affects plasma characteristics as coil current increases at a 0.2 torr pressure constant. Coil currents changed the discharge zone glow in the cylinder design. The photos indicated that plasma particles absorb more energy as AC frequency increases, increasing light emission brightness. The usual glow discharge areas created by applied AC voltage resemble DC discharge at all AC frequencies studied. Cylinder shape affects glow area size and shape. Additionally, plasma characteristics rise with coil current at all AC frequencies under study. The magnetic field's axial profile shows that both configurations have maximum values at the inner electrode extremities and minimum values in the center rising plasma and electron frequencies. Due to plasma confinement, magnetic fields enhance electron temperature, density, and Debye length.

References

[1] P.V Kashtanov, B.M. Smirnov and R. Hippler, “Magnetron plasma and nanotechnology,” *Physics-Uspekhi*, 50(5) (2007) 455.

[2] S.D. Ekpe et al., “Effect of magnetic field strength on deposition rate and energy flux in a dc magnetron sputtering system”, *J. Vac. Sci. Technol. A Vac. Surf. Film.*, 27(6) (2009) 1275-1280.

[3] G.A. Bleykher et al., “Energy and substance transfer in magnetron sputtering systems with liquid-phase target”, *Vacuum*, 124 (2016) 11-17.

[4] G. Zhou et al., “Influence of magnetic field configuration on plasma characteristics and thin film properties in dual magnetron reactive high power impulse magnetron sputtering discharge with Al in Ar/O_2 mixture”, *Surf. Coat. Technol.*, 409 (2021) 126837.

[5] D.M. Mattox and V.H. Mattox, **"Vacuum Coating Technology"**, Springer (2003).

[6] G.O. Este and W.D. Westwood, “AC and RF reactive sputtering”, in **Handbook of Thin Film Process Technology**, CRC Press (2018), pp. A5-2.

[7] D.A. Glocker, **"Handbook of Thin Film Process Technology"**, 98/1 Reactive Sputtering, CRC Press (2018).
[8] J. Musil et al., "Reactive magnetron sputtering of thin films: present status and trends", *Thin Solid Films*, 475(1-2) (2005) 208-218.
[9] S.N. Mazhir et al., "Texture Analysis of smear of Leukemia Blood Cells after Exposing to Cold Plasma", *Baghdad Sci. J.*, 14(2) (2017) 403-410.
[10] M.K. Khalaf et al., "Influence of nanocrystalline size on optical band gap in CdSe thin films prepared by DC sputtering", *Photon. Nanostruct. Fund. Appl.*, 18 (2016) 59-66.
[11] M.K. Khalaf et al., "Influence of RF sputtering power on surface properties and biocompatibility of 316L stainless steel alloy by deposition of TiO_2 thin films", *Mater. Res. Exp.*, 6(3) (2018) 35401.
[12] O.A. Hammadi, "New technique to synthesize silicon nitride nanopowder by discharge-assisted reaction of silane and ammonia", *Mater. Res. Exp.*, 8(8) (2021) 085013.
[13] S.N. Mazhir et al., "A Study of Plasma parameters in gold sputtering System by Means of Optical Emission Spectroscopy", *IOP Conf. Ser.: Mater. Sci. Eng.*, 871(1) (2020) 12081.
[14] C. Aragón and J.A. Aguilera, "Characterization of laser induced plasmas by optical emission spectroscopy: A review of experiments and methods", *Spectrochim. Acta B: At. Spectrosc.*, 63(9) (2008) 893-916.
[15] M.A. Gondal and T. Hussain, "Determination of poisonous metals in wastewater collected from paint manufacturing plant using laser-induced breakdown spectroscopy", *Talanta*, 71(1) (2007) 73-80.
[16] S.K. Taha, S.N. Mazhir and M.K. Khalaf, "A Comparative Study on the Electrical Characteristics of Generating Plasma by Using Different Target Sources", *Baghdad Sci. J.*, 15(4) (2018) 436-440.
[17] K.A. Aadim, "Spectroscopic study for plasma parameters in co-sputtering system", *Iraqi J. Phys.*, 14(31) (2019) 122-128.
[18] B. Denis et al., "Plasma sterilization of pharmaceutical products: from basics to production", *Plasma Process. Polym.*, 9(6) (2012) 619-629.
[19] N. Idris et al., "Temperature estimation using Boltzmann plot method of many calcium emission lines in laser plasma produced on river clamshell sample", *IOP J. Phys.: Conf. Ser.*, 1120(1) (2018) 12098.
[20] Q.A. Abbas, "Influence of the Distance between Focusing Lens and Target Surface on the Characteristics of Laser-excited Lead Plasma", *Iraqi J. Sci.*, 62(12) (2021) 4694-4701.
[21] N. Ohno et al., "Validity of electron temperature measurement by using Boltzmann plot method in radio frequency inductive discharge in the atmospheric pressure range", *Plasma Fusion Res.*, 1 (2006) 28.
[22] M.M. Shehab and K.A. Aadim, "Spectroscopic diagnosis of the CdO:CoO plasma produced by Nd:YAG laser", *Iraqi J. Sci.*, 62(9) (2021) 2948-2955.
[23] S. Waheed et al., "Effect of magnetic field on laser induced breakdown spectroscopy of zirconium dioxide (ZrO_2) plasma", *Optik*, 140 (2017) 536-544.
[24] Q.A. Abbas, "Influence of working pressure and lasing energy of Al plasma in laser-induced breakdown spectroscopy", *Iraqi J. Phys.*, 17(40) (2019) 59-66.
[25] S.F. Khaleel and Q.A. Abbas, "Influence of Dielectric Media on the Plasma Characteristics in DBD Discharge", *Iraqi J. Sci.*, 63(6) (2022) 2470-2481.
[26] M.M. Kadhim, Q.A. Abbas and M.R. Abdulameer, "Study of some plasma characteristics in dielectric barrier discharge (DBD) system", *Iraqi J. Sci.*, 63(5) (2022) 2048-2056.
[27] A.K. Bard and Q.A. Abbas, "Influence of Cylindrical Electrode Configuration on Plasma Parameters in a Sputtering System", *Iraqi J. Sci.*, 63(8) (2022) 3412-3423.
[28] Q.A. Abbas, A.F. Ahmed and F.A.-H. Mutlak, "Spectroscopic analysis of magnetized hollow cathode discharge plasma characteristics", *Optik*, 242 (2021) 167260.
[29] S.M. Fathi and S.J. Kadhim, "Optical Emission Spectroscopy for Studying Fe Plasma Parameters Produced by Exploding Wire Technique in Carbon Nanotubes - Water Colloid", *Iraqi J. Sci.*, 63(1) (2022) 163-169.
[30] N.K. Hussein and S.J. Kadhem, "Spectroscopic Diagnosis of Arc Carbon and Magnesium Plasma", *Iraqi J. Sci.*, 63(6) (2022) 2492-2501.
[31] M.J. Ketan and K.A. Aadim, "Characteristics of Lead and Sulfur Plasma Parameters by Optical Emission Spectroscopy", *Iraqi J. Sci.*, 64(1) (2023) 188-196.
[32] K.A. Aadim, "Effect of Argon and oxygen pressure on Zn magnetron plasma produced by RF power supply", *Iraqi J. Phys.*, 15(34) (2017) 65-71.
[33] A.F. Ahmed and A.A. Yousef, "Spectroscopic Analysis of DC-Nitrogen Plasma Produced using Copper Electrodes", *Iraqi J. Sci.*, 62(10) (2021) 3560-3569.
[34] M. Fikry, W. Tawfik and M.M. Omar, "Investigation on the effects of laser parameters on the plasma profile of copper using picosecond laser induced plasma spectroscopy", *Opt. Quantum Electron.*, 52 (2020) 1-16.
[35] A.F. Ahmed et al., "Plasma parameters of Au nano-particles ablated on porous silicon produced via Nd:YAG laser at 355 nm for sensing NH_3 gas", *Optik*, 249 (2022) 168260.
[36] S.E. Abdulghani and Q.A. Abbas, "Influence of Fe_2O_3 Dust Particles on the Plasma Characteristics of D.C Sputtering System", *Iraqi J. Sci.*, 63(7) (2022) 2945-2954.
[37] A.K. Bard and Q.A. Abbas, "Influence of cylindrical magnetron sputtering configurations on plasma characteristics", *Optik*, 272 (2023) 170346.

[38] K.A. Aadim, K.A. Ahmed and R.S. Mohammed, "Diagnostic analysis of Cu and CuZn plasma produced by Nd: YAG nanosecond laser at 1064 nm", in *Proc. 2nd Int. Conf. Phys. Sci. Adv. Mater., Turkey* (2021).
[39] M.A. Essa and K.A. Aadim, "Spectroscopic studying of plasma parameters for SnO_2 doped ZnO prepared by pulse Nd:YAG laser deposition", *Iraqi J. Phys.*, 17(42) (2019) 125-135.
[40] R.N. Muhsin and K.A. Aadim, "Spectroscopic study performance of laser produced $CdTe_{(x)}:S_{(1-x)}$ plasma", 17(42) (2019) 96-102.
[41] M.A. Mohammed, H.N. Hashim and K.A. Aadim, "Analytical diagnostics of Zr, ZnO and $Zr_{(1-x)}:ZnO_{(x)}$ plasma produced by laser", *J. Opt.*, (2023) 1-8, doi: 10.1007/s12596-023-01264-0.
[42] H.I. Hussein and K.A. Aadim, "Spectroscopic Study of Plasma Parameters Produced by Pin-Plate DC Discharge Technique", *Iraqi J. Sci.*, 63(3) (2022) 971-976.
[43] M.A. Khalaf, B.M. Ahmed and K.A. Aadim, "Spectroscopic analysis of $CdO_{1-X}:Sn_X$ plasma produced by Nd:YAG laser", *Iraqi J. Sci.*, 61(7) (2020) 1665-1671.
[44] A.K. Abbas, K.A. Aadim and M.F. Jawaad, "Spectroscopic diagnostic of (Zn:NiO) plasma by laser induced breakdown spectroscopy", in *AIP Conf. Proc.*, 2372(1) (2021) 80013.
[45] R.S. Mohammed, K.A. Aadim and K.A. Ahmed, "Spectroscopy Diagnostic of Laser Intensity Effect on Zn Plasma Parameters Generated by Nd:YAG Laser", *Iraqi J. Sci.*, 63(9) (2022) 3711-3718.
[46] K.A. Aadim, A.A.K. Hussain and W.I. Yaseen, "Diagnostics of low-pressure capacitively coupled RF discharge argon plasma", *Iraqi J. Phys.*, 13(27) (2015) 76-82.
[47] M.M. Kadhim and Q.A. Abbas, "The Influence of the Magnetic Field on the Plasma Characteristics in Hollow Electrodes Discharge System", *Iraqi J. Sci.*, 63(10) (2022) 4254-4266.
[48] O.A. Hamadi, "Characteristics of CdO-Si heterostructure produced by plasma-induced bonding technique", *Proc. IMEchE L: J. Mater. Des. Appl.*, 222(1) (2008) 65-71.
[49] K.A. Aadim, "Spectroscopic study the plasma parameters for Pb doped CuO prepared by pulse Nd:YAG laser deposition", *Iraqi J. Phys.*, 16(38) (2018) 1-9.
[50] J. Kramida, A. Ralchenko and Yu. Reader, "NIST ASD Team", NIST@Spectra Database (ver. 5.10) (2022), doi: https://doi.org/10.18434/T4W30F.

Table (2) The effect of AC frequency on the discharge parameters in different coil currents

Coil current (A)	Electron Temperature (eV)	Electron Number Density×10^{16} (cm^{-3})	Debye Length ×10^{-6} (cm)	Plasma Parameter
7 kHz				
0	0.67499	7.557434963	2.220497425	3478
2	0.70328	7.9908326	2.204230112	3597
4	0.79643	8.564492875	2.265748979	4187
6	0.84452	8.73083565	2.310818718	4528
9 kHz				
0	0.76693	8.051639588	2.293108022	4081
2	0.83514	9.863190725	2.162020168	4190
4	0.88044	9.885766738	2.217346256	4530
6	0.90163	9.968163025	2.234577515	4675

